# Evaluation of Surgical Margins with Intraoperative PSMA PET/CT and Their Prognostic Value in Radical Prostatectomy

Moraitis, Alexandros; Kahl, Theresa; Kandziora, Jens; Jentzen, Walter; Kersting, David; Püllen, Lukas; Reis, Henning; Köllermann, Jens; Kesch, Claudia; Krafft, Ulrich; Hadaschik, Boris A; Zaidi, Habib; Herrmann, Ken; Barbato,&nbspFrancesco [**and 3 more**]

**How to cite**

MORAITIS, Alexandros et al. Evaluation of Surgical Margins with Intraoperative PSMA PET/CT and Their Prognostic Value in Radical Prostatectomy. In: The Journal of nuclear medicine, 2025, vol. 66, n° 3, p. 352–358. doi: 10.2967/jnumed.124.268719

This publication URL: https://archive-ouverte.unige.ch/unige:183622

Publication DOI: 10.2967/jnumed.124.268719

# Evaluation of Surgical Margins with Intraoperative PSMA PET/CT and Their Prognostic Value in Radical Prostatectomy

Alexandros Moraitis*[1,2], Theresa Kahl*[2,3], Jens Kandziora[1,2], Walter Jentzen[1,2], David Kersting[1,2], Lukas Püllen[2,3], Henning Reis[4], Jens Köllermann[4], Claudia Kesch[2,3], Ulrich Krafft[2,3], Boris A. Hadaschik[2,3], Habib Zaidi[5], Ken Herrmann[1,2], Francesco Barbato[1,2], Wolfgang P. Fendler[1,2], Christopher Darr*[2,3], and Pedro Fragoso Costa*[1,2]

[1]*Department of Nuclear Medicine, West German Cancer Center, University Hospital Essen, University of Duisburg-Essen, Essen, Germany;* [2]*German Cancer Consortium, Partner Site University Hospital Essen, Essen, Germany;* [3]*Department of Urology, University Hospital Essen, Essen, Germany;* [4]*Dr. Senckenberg Institute of Pathology, University Hospital Frankfurt, Frankfurt, Germany; and* [5]*Division of Nuclear Medicine and Molecular Imaging, Geneva University Hospital, Geneva, Switzerland*

Detection of positive resection margins in surgical procedures of high-risk prostate cancer is key for minimizing the risk of recurrence. This study aimed at evaluating the accuracy of functional tumor-volume segmentation in intraoperative ex vivo PET/CT for margin assessment in prostate cancer patients undergoing radical prostatectomy. **Methods:** Seven high-risk prostate cancer patients received [$^{18}$F]PSMA-1007 before radical prostatectomy. After removal of the prostate gland, ex vivo imaging on the AURA 10 PET/CT system was performed, and functional tumor volume was segmented using 4 semiautomatic segmentation methods. Resection margins and volumes were compared with histopathology. Additionally, a supportive phantom study was conducted to assess segmentation accuracy at low radiopharmaceutical activity. **Results:** Clinically, 18 lesions were analyzed in intraoperative PET/CT. Sensitivity, specificity, and positive and negative predictive values of margin detection were 83%, 100%, 100%, and 92%, respectively, using an iterative thresholding method. In 1 patient, a biochemical recurrence was observed within 1 y of prostate-specific antigen follow-up, and 1 patient underwent adjuvant radiotherapy. The remaining 5 patients were still undergoing prostate-specific antigen follow-up with no evidence of biochemical recurrence. On the basis of a phantom-deduced minimal segmentable activity concentration of approximately 2 kBq/mL, we propose an administered [$^{18}$F]PSMA-1007 activity of at least 1.9 and 0.4 MBq/kg for preoperative and intraoperative injections, respectively. **Conclusion:** Intraoperative ex vivo PET/CT is a promising modality for intraoperative margin assessment. Prospective trials are needed to further investigate the value of specimen PET/CT-based radioguided surgery in high-risk prostate cancer.

**Key Words:** margin assessment; PET/CT; prostate cancer; radical prostatectomy; radioguided surgery

**J Nucl Med 2025; 66:352–358**
DOI: 10.2967/jnumed.124.268719

In men, prostate cancer (PC) is the most prevalent type of cancer worldwide and is projected to see significant increases in both incidence and mortality rates over the next 2 decades, which poses the need for adequate treatment options (*1,2*). These include radical prostatectomy (RP) or radiotherapy of the prostate in combination with androgen deprivation therapy (*3*).

In RP, positive surgical margins (PSMs) are associated with an increased risk of developing biochemical recurrence or metastases. PSMs occur in 11%–38% of patients undergoing RP, whereas the effect of PSMs is strongly influenced by stage, length, number, and location of PSMs, as well as by the surgical approach and surgeon experience (*4,5*).

At present, several techniques have evolved to optimize surgical margin assessment. Intraoperative frozen section biopsy has proven to significantly reduce PSMs with even better outcomes when combined with preoperative imaging, such as multiparametric MRI (*4,6*). Other novel approaches are based on detection of the prostate-specific membrane antigen (PSMA). PSMA expression is upregulated in over 90% of PC patients, which makes PSMA a sensitive marker for PC detection (*7,8*). Gondoputro et al. (*9*) used preoperative SPECT in conjunction with intraoperative γ-probes to improve the detection of lymph node metastases during RP and reported a sensitivity of 76%. In total, 90% of false-negative lymph nodes were reported to be micrometastases (≤3 mm) (*9*). Other studies investigating the accuracy of γ-probes in detecting cancerous tissue in lymph nodes in either a primary or secondary setting reported similar sensitivities ranging from 50% to 87.5% (*10–14*). In parallel, the detection of $\beta^+$-emitters has gained increasing interest over the last decade (*15–17*). Collamati et al. (*18*) used a β-probe after intraoperative injection of [$^{68}$Ga]Ga-PSMA-11 during RP. Although sensitive to detection, the probe failed to reliably differentiate between PSM and close surgical margins (<1 mm). More specifically, in 5 of 7 patients showing increased uptake, only 2 PSMs (40%) were confirmed histologically. The use of β-emitters to allow for intraoperative optical light imaging via Cherenkov luminescence in the context of RP has also been reported with sensitivities ranging from 60% to 83% (*19–22*). Improved specificity in Cherenkov luminescence was obtained using a short-pass filter to minimize the rate of false positives (*19*). The applicability of flexible autoradiography–enhanced Cherenkov luminescence was also investigated using PSMA-labeled $\beta^+$-emitters for intraoperative margin assessment on prostate

Received Aug. 29, 2024; revision accepted Jan. 6, 2025.
For correspondence or reprints, contact Pedro Fragoso Costa (pedro.fragoso-costa@uni-due.de).
*Contributed equally to this work.
Published online Feb. 6, 2025.

specimens in high-risk PC patients and achieved moderate outcomes while both PSMs were not detected (*23*). In summary, all of these modalities appear to be restricted in their clinical application by either low sensitivity or poor spatial resolution. The latter is particularly evident in the inability to distinguish PSMs from close surgical margins as well as missing microscopic lesions.

Because of its high sensitivity and specificity, PSMA PET has been established for staging high-risk and biochemically recurrent PC and has been incorporated into guidelines for primary staging of high-risk PC (*24–26*).

The first high-resolution ex vivo PET/CT system (AURA 10; XEOS Medical NV) dedicated for the operating room was recently used in PC patients undergoing RP. Promising results using [$^{68}$Ga]Ga-PSMA-11 for intraoperative assessment of surgical margins in prostate specimens as well as good correlation with histopathology were recently published (*27,28*). In perspective, the increasing availability of [$^{18}$F]PSMA-1007 and other novel $^{18}$F-labeled tracers might facilitate PET/CT-based margin assessment because of higher PET spatial resolution (lower positron energy) and higher signal intensity (higher positron yield and higher physical half-life) of $^{18}$F compared with $^{68}$Ga (*29,30*).

In intraoperative margin assessment, the exact reproduction of tumor-volume boundaries is of utmost importance. However, delineation of cancer foci and quantification of PSMA-positive tumor volume in PET/CT images are highly dependent on the method used for volume segmentation (*31*). Several methods have been proposed based on percentage thresholding of maximal uptake values, fixed thresholding, and histogram-based or local-adaptive algorithms (*31–34*). To date, no recommendation exists on standardized volume segmentation in PSMA PET imaging. In addition, heterogeneous lesion uptake, lesion geometry, and size as well as image reconstruction parameters and count statistics may affect the accuracy of volume segmentation depending on the method used.

The main objective of this study was to evaluate the accuracy of intraoperative margin assessment in ex vivo [$^{18}$F]PSMA-1007 PET/CT imaging in the context of RP using several segmentation methods.

## MATERIALS AND METHODS

Surgical margins in intraoperative ex vivo [$^{18}$F]PSMA-1007 PET/CT imaging were evaluated in a 2-step process. Functional tumor volumes obtained with 4 volume segmentation methods on prostate specimens after RP were compared with histopathologic analysis to assess the agreement of surgical margin findings. Surgical margins and tumor volumes were also compared with prostate-specific antigen (PSA) follow-up data. In a consecutive phantom study, the accuracy of the volume segmentation approaches was validated for a phantom mimicking the prostate gland and with spheric lesions of known activity and volume. Based on these measurements, recommendation on the injected activities for intraoperative PET/CT was made for different procedural scenarios.

### Patients and Clinical Setup

The study was conducted in accordance with the Declaration of Helsinki and approved by the local Ethics Committee of University Duisburg-Essen, Medical Faculty (protocol code: 23-11124-BO). Informed consent was obtained from all subjects involved in the study. From January 2023 to August 2023, 7 men with histologically confirmed, high-risk PC eligible for RP were enrolled. All patients had high-risk features, including at least 1 of either a PSA concentration of 20 ng/mL or more within 12 wk before RP, an International Society of Urological Pathology grades 3–5, or a clinical stage T3 or worse. Participants received a median of 3.7 MBq/kg (range, 3.2–4.8 MBq/kg) of [$^{18}$F]PSMA-1007 on the day of surgery. [$^{18}$F]PSMA-1007 was produced according to the German Pharmaceuticals Act §13(2b). After a median of 1.3 h (range, 0.8–1.6 h) after injection, routine PET/CT ($n = 4$) or PET/MR ($n = 2$) was performed and reviewed by experienced nuclear medicine physicians to exclude high-volume or metastatic disease. For 1 patient who received clinical PET/CT a few weeks before RP, clinical PET imaging on the day of surgery was not performed. The second version of the standardized evaluation of molecular imaging in PC (PROMISEv2) was used for the analysis and reporting of PSMA PET findings (*35*). Thereafter, RP and extended pelvic lymphadenectomy were performed by an experienced surgeon with more than 500 cases. Prostatectomy was always performed before lymphadenectomy to minimize the time between tracer injection and intraoperative ex vivo PET/CT imaging of the prostate specimen. PET/CT imaging was followed by histologic analysis (details are in the Histopathologic Analysis section). For all patients, PSA data were collected before and regularly after surgery in an outpatient follow-up setting. A conceptual illustration of the clinical setup is shown in Figure 1. Detailed patient and imaging characteristics are provided in Table 1.

### Ex Vivo PET/CT Imaging

After RP, the whole prostate gland was placed on a dedicated specimen container (dorsal peripheral zone on the bottom) and scanned intraoperatively on the AURA 10 ex vivo PET/CT system. The median time between tracer injection and imaging was 4.6 h (range, 4.3–6.3 h). The AURA 10 consists of a high-resolution CT and a PET component with 22 monolithic lutetium–yttrium oxyorthosilicate detector crystals arranged in 2 rings. Its field of view of 6 cm and 10 cm in the axial and transaxial direction, respectively, was large enough to capture the whole specimen. As per clinical standard protocol, the CT was acquired first (50 kVp, 0.6 mA, 512 projections) and used for attenuation correction and anatomic correlation, followed by a 10-min PET acquisition. Attenuation-corrected PET images were reconstructed into a 252 × 252 transverse matrix with cubic voxels of 0.4 mm$^3$ in size using a 3-dimensional maximum likelihood expectation maximization algorithm with 20 iterations. For $^{18}$F, the axial and transaxial image-based spatial resolution for these settings was reported to be 1.77 mm and 1.87 mm, respectively (*36*).

### Tumor Segmentation and Image Analysis

PSMA-positive lesions on PET/CT were segmented using several semiautomated approaches. They were applied on volumes of interest that were drawn manually for each lesion, large enough to surround the whole lesion, but excluding off-target PSMA-positive regions. The following segmentation approaches were used:

- Percentage thresholding 1: 30% threshold ($V_{30\%}$), based on preliminary evaluations of our working group on the AURA 10 PET/CT system (*37*).
- Percentage thresholding 2: 41% threshold ($V_{41\%}$) as suggested by Draulans et al. (*33*) for clinical [$^{18}$F]PSMA-1007 PET segmentation.
- Fixed SUV thresholding: A fixed SUV of 4, as previously proposed to resample tumor volume ($V_{SUV=4}$) in clinical [$^{18}$F]PSMA-1007 PET imaging (*34*). Due to imaging time delay, the imaged activity concentration from ex vivo PET/CT was decay corrected to the time of clinical imaging approximately 1 h after injection.
- Iterative thresholding: A sophisticated method developed by Jentzen (*38*) that takes into account the mean activity concentration in the lesion and the surrounding background to estimate its volume iteratively based on a sphere model ($V_{iterative}$).

The spatial resolution of the PET/CT scanner was used to define the minimum positive area for a PET-based PSM. More specifically,

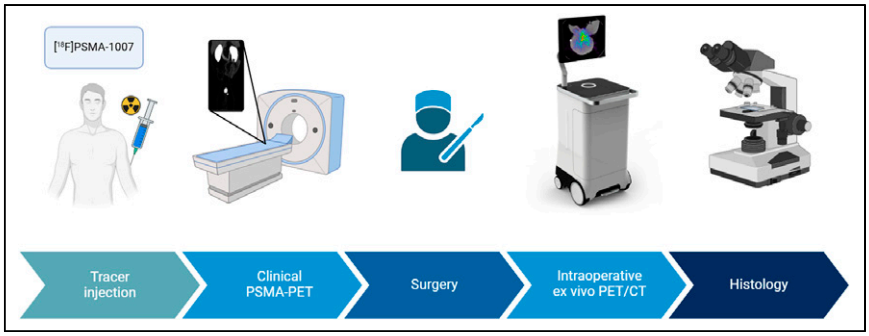


**FIGURE 1.** Clinical setup.

PET-based PSM was denoted when the area of the segmented tumor crossing the anatomic boundaries of the prostate specimen was at least 2.56 $mm^2$. This equals approximately 4 × 4 voxels and corresponds to the surface resolution of the AURA 10 PET/CT system when using $^{18}F$ (*36*). Figure 2 illustrates the principle for a point source.

The clinical performance of the segmentation methods was evaluated with regards to PSM detection in terms of sensitivity, specificity, positive predictive value, negative predictive value, and accuracy (*39*).

### Histopathologic Analysis

Pathologic work-up was performed according to current clinical standards by dedicated pathologists with more than 10 y of experience in genitourinary pathology. For the analysis, quarters were digitally reconstructed to whole mounts to determine the dimensions of the tumor in 3 planes.

### Performance of Ex Vivo PET/CT: Phantom Evaluation

To validate the clinical results, a phantom study was performed focusing on the accuracy of volume segmentation methods under clinical conditions. The phantom consisted of a cylindric background region with spheric inserts of 0.2, 0.5, 1.0, and 2.0 mL volume representing reference lesions. Only 1 sphere at a time was inserted. Spheres were filled with around 20 kBq/mL of $^{18}F$-containing solution, which represents the upper limit of observed activity concentrations in prostate lesions at the time of imaging. A sphere-to-background ratio of 8 was used, again, on the basis of the observations in prostate specimens. The phantom was scanned using the same acquisition and reconstruction parameters as used for clinical imaging. In addition, a decay series with the 1-mL sphere was performed, in which the phantom was scanned over several half-lives until the activity concentration was below 1 kBq/mL and the sphere was no longer discernible from the background.

The accuracy of volume segmentation was evaluated in terms of percent deviation from the actual sphere volume (obtained gravimetrically) and by Dice similarity coefficient analysis (*40*). The Dice similarity coefficient is a measure of the spatial overlap between a segmented volume ($V_i$) using segmentation method $i$ and its surrogate ground truth ($V_{true}$) given as:

$$DSC(V_i, V_{true}) = 2 \cdot \frac{V_i \cap V_{true}}{V_i + V_{true}}, \qquad \text{Eq. 1}$$

where $|V_i \cap V_{true}|$ denotes the overlap of the volumes and is referred to as the true-positive volume fraction. The Dice similarity coefficient is a useful metric for quantification of lesion-volume boundaries in surgical margin assessment (*41*).

### Software and Statistical Analysis

Tumor volumes and PSMs were obtained and analyzed using PMOD 4.2. software (PMOD Technologies Ltd.). Statistical analysis was performed with SPSS statistic software, version 26 (IBM). Categoric variables were summarized with proportions. Spearman correlation and paired Wilcoxon signed-rank tests were used to correlate PSM between PET/CT and histopathology and to compare tumor volumes obtained with different segmentation methods, respectively, and significance was assumed for $P$ values of less than 0.05.

## RESULTS

### Comparison of Segmented Tumor Volumes

A total of 18 lesions from 7 patients were analyzed in intraoperative ex vivo PET/CT. Figure 3 illustrates the distribution of lesion volumes for all segmentation methods. Lesion volumes obtained with a $V_{41\%}$ were significantly smaller compared with the other methods ($P < 0.01$). In addition, volumes differed significantly between $V_{30\%}$ and $V_{iterative}$ ($P = 0.018$).

A representative example of a lesion (Fig. 4A), as well as the lesion with largest differences among segmentation methods (Fig. 4B), is illustrated in Figure 4. For the latter, the maximum activity concentration was 53 kBq/mL, whereas the maximum-to-mean lesion activity concentration ratio was 1.9, 2.6, 3.5, and 4.3 for

**TABLE 1**
Patients and Imaging Characteristics

| Patient | Age (y) | BMI | Initial PSA (ng/mL) | miTNM codeline | Gleason score | R-status* | Prostate volume (mL) | Injected activity (MBq) | Time to clPET/CT (h) | Time to iPET/CT (h) |
|---|---|---|---|---|---|---|---|---|---|---|
| 1 | 62 | 23.5 | 5.48 | miT3a N0 M0 | 9 | R1 (1) | 42 | 375 | 0.77 | 4.60 |
| 2 | 80 | 29.0 | 19.0 | miT2m N0 M0 | 9 | R0 | 123 | 347 | 1.43 | 6.27 |
| 3 | 60 | 23.4 | 16.5 | miT2m N0 M0 | 7a | R0 | 51 | 256 | 1.40 | 4.93 |
| 4 | 70 | 28.7 | 6.90 | miT2u N0 M0 | 8 | R0 | 82 | 299 | 0.97 | 4.30 |
| 5 | 67 | 22.2 | 8.27 | miT3a N0 M0 | 9 | R1 (2) | 42 | 350 | 1.18 | 4.55 |
| 6 | 68 | 27.1 | 6.33 | miT3b N1 M0 | 9 | R1 (3) | 39 | 350 | — | 4.63 |
| 7 | 69 | 27.0 | 4.93 | miT2m N0 M0 | 8 | R0 | 49 | 259 | 1.62 | 4.87 |

*Numbers within parentheses denote number of individual lesions with R1 status.

BMI = body mass index; miTNM = molecular imaging TNM according to PROMISEv2; clPET/CT = clinical PET/CT; iPET/CT = intraoperative ex vivo PET/CT.

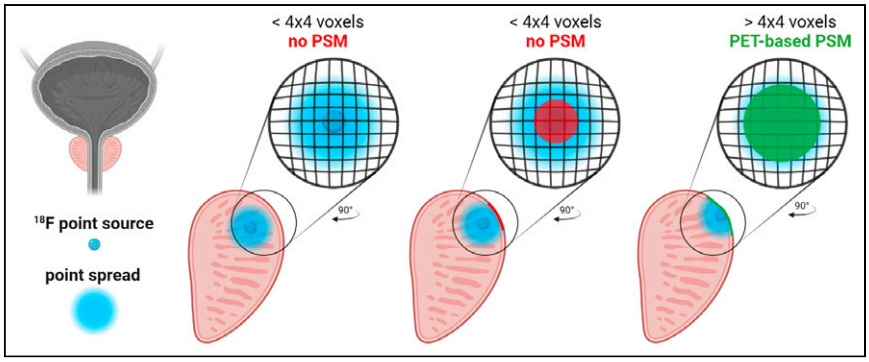


**FIGURE 2.** Conceptual illustration of PET-based PSM. For $^{18}$F, PSM is considered when signal crossing physical boundaries of prostate specimen equals at least 2.56 mm$^2$ (≙ 4 × 4 voxels) based on spatial resolution of AURA 10 PET/CT.

$V_{41\%}$, $V_{30\%}$, $V_{SUV=4}$, and $V_{iterative}$, respectively, indicating a highly inhomogeneous activity distribution.

### Comparison with Histopathology

Table 2 lists the performance of intraoperative [$^{18}$F]PSMA-1007 ex vivo PET/CT imaging for detecting PSMs in PSMA-positive lesions in prostate specimens. Five of 6 histopathologically confirmed PSMs were detected in PET/CT imaging when using iterative thresholding. Diameter of the PET/CT-based PSMs ranged from 2.8 to 11.6 mm (area, 5 mm$^2$ to 0.6 cm$^2$) and correlated excellently (correlation coefficient = 0.90, $P < 0.001$) with histopathology. The 1 PSM that tested negative in ex vivo PET/CT imaging showed no uptake on the CT-based physical boundaries of the specimen despite histopathologically confirmed PSM of 10-mm diameter. Specificity and positive predictive value were up to 100% (for $V_{41\%}$ and $V_{iterative}$). Negative predictive value and accuracy were highest using $V_{30\%}$ (85% and 83%, respectively) and $V_{iterative}$ (92% and 94%, respectively). Examples for the comparison of intraoperative PET/CT margin assessment and histopathologic findings are illustrated in Figure 5 for 2 cases: true-positive surgical margin and false-negative surgical margin in PET/CT.

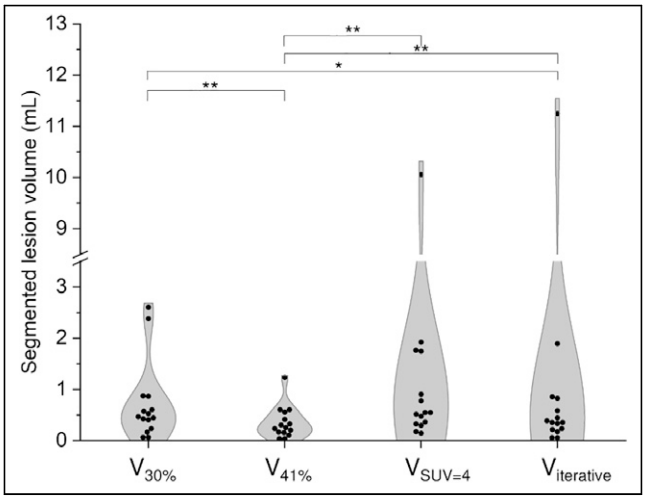


**FIGURE 3.** Violin plot of volume distribution of intraprostatic lesions segmented using different functional tumor-volume segmentation methods. Significant paired differences are marked with * for $P \leq 0.05$ and ** for $P \leq 0.01$.

### Follow-up

Postoperatively, depending on the risk and stage, additional radiotherapy with androgen deprivation therapy for 6 mo or PSA-controlled follow-up was recommended. Results are summarized in Supplemental Table 1 (supplemental materials are available at http://jnm.snmjournals.org). In the 3 patients with PSM, adjuvant radiotherapy was recommended, alternatively with a PSA follow-up. Initially, 1 patient opted for adjuvant radiotherapy, and the remaining 2 patients opted for PSA follow-up. One patient developed an increase in PSA after RP, resulting in early radiotherapy due to biochemical recurrence. The remaining 5 patients underwent follow-up with PSA measurements at quarterly intervals. As of March 2024, there was no evidence of biochemical or local recurrence in these 5 patients.

### Performance of Ex Vivo PET/CT: Phantom Evaluation

Scanner performance was evaluated using the clinical imaging protocol to study segmentation accuracy under controlled conditions. Figure 6 illustrates the agreement of volume segmentation for various lesion sizes; all segmentation methods yielded a ±20% result for the 2-mL reference lesion. However, for smaller volumes (Fig. 6A) and lower activity concentration (Fig. 6B), segmentation within a tolerance of ±20% was obtained only with $V_{30\%}$ and $V_{iterative}$. The Dice similarity coefficients are listed in Supplemental Tables 2 and 3. Based on the decay series on the 1-mL reference lesion, the minimum segmentable activity concentration was approximately 2 kBq/mL (condition 1).

*Recommendation on Injected Activity.* In a clinical setting, the lesion activity depends both on the administered activity to the patient and the elapsed time for specimen scanning. For those variables, we calculated the minimal activity to be administered for reliable margin assessment assuming an average [$^{18}$F]PSMA-1007 prostate uptake of 0.13% (data from clinical PET/CT (*30*); condition 2). Two time intervals were considered (at 2 and 6 h after injection) to mimic intraoperative and 1-stop-shop clinical protocols in RP, respectively (condition 3). To comply with this specific set of conditions (at 95% CI), we recommend the administration

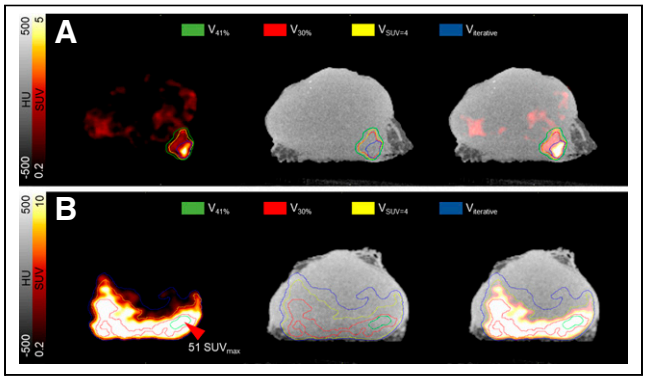


**FIGURE 4.** Functional tumor-volume segmentation for representative lesion (A) and lesion with highest discrepancies among segmentation methods (B). Axial slice is shown in PET (left) and CT (middle) imaging, as well as fused PET/CT image (right). HU = Hounsfield unit.

**TABLE 2**
Performance of Intraoperative [$^{18}$F]PSMA-1007 Ex Vivo PET/CT in PSM Detection in Prostate Specimens (Histopathology Serving as Reference)

| Parameter | Segmentation method | | | |
|---|---|---|---|---|
| | $V_{30\%}$ | $V_{41\%}$ | $V_{SUV=4}$ | $V_{iterative}$ |
| Sensitivity (%) | 67 | 33 | 50 | 83 |
| Specificity (%) | 92 | 100 | 92 | 100 |
| PPV (%) | 80 | 100 | 75 | 100 |
| NPV (%) | 85 | 75 | 79 | 92 |
| Accuracy (%) | 83 | 78 | 78 | 94 |

PPV = positive predictive value; NPV = negative predictive value.

of at least 0.4 and 1.9 MBq/kg for intraoperative and preoperative injections, respectively.

## DISCUSSION

In high-risk PC, reliable intraoperative margin assessment is key for guiding RP to potentially reduce the risk of disease progression and delay the need for additive radiotherapy (*4*). Our study demonstrated the feasibility of intraoperative ex vivo PET-based margin assessment with [$^{18}$F]PSMA-1007.

Of 19 histopathologically confirmed lesions, 18 were detected in ex vivo PET/CT, which is in line with the reported 91% detection rate for intraprostatic lesions in clinical PSMA PET/CT imaging (*42*). At the current pilot stage of intraoperative PET/CT imaging, the surgical approach was not adjusted to PET data. Volume segmentation and image analysis were performed retrospectively to allow for comparison with histopathology. However, the reported sensitivity of 83% and specificity of 100% for PSM identification, when using iterative thresholding, demonstrate encouraging potential for PET-based radioguided surgery in RP.

Muraglia et al. (*27*) were the first to report on intraoperative ex vivo PET/CT images using the AURA 10 specimen imager in 2 high-risk PC patients injected with [$^{68}$Ga]Ga-PSMA-11 and identified 1 PSM from visual inspection that was later confirmed by

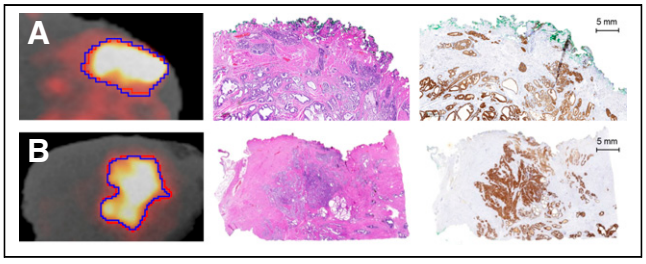


**FIGURE 5.** Histopathologically confirmed PSMs compared with images from intraoperative ex vivo PET/CT with segmented tumor volumes using $V_{30\%}$ (red) and $V_{iterative}$ (blue) method. (A) Patient 1, basal right; (B) patient 5, basal right. Histologic images in middle are hematoxylin and eosin stained with tumor cell glands or clusters at thermally altered and inked surgical margin. Immunohistochemical microphotographs on right show pan cytokeratin stainings, highlighting epithelial structures in gland and at surgical margin.

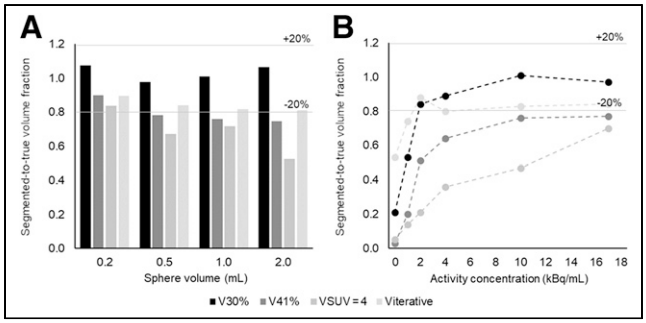


**FIGURE 6.** Phantom evaluation. (A) Volume dependency of segmentation accuracy for all segmentation methods. (B) Dependency of segmentation accuracy on activity concentration (in kBq/mL) for 1-mL spheric reference lesion.

histopathologic analysis. Our group previously performed intraoperative PET/CT in 10 high-risk PC patients during RP after injection of either [$^{68}$Ga]Ga-PSMA-11 or [$^{18}$F]PSMA-1007 and reported an overall lesion detection rate of 93% when compared with multiparametric MRI and whole-body preoperative PSMA PET (*28*). Our recent study expands on these findings and investigated the accuracy of easily implementable semiautomatic functional tumor-volume segmentation methods to facilitate objective margin assessment. Iterative thresholding performed best in terms of sensitivity, specificity, and positive and negative predictive values for PSMs. This was also in line with our observations on phantom data. Phantom-deduced volume accuracy of less than ±20% was only obtained with $V_{30\%}$ and $V_{iterative}$. A 20% deviation in a 1-mL spherically shaped lesion corresponds to a deviation in the radius of less than 1 voxel size (=0.4 mm).

The spatial resolution of the reconstructed PET images is, indeed, a limiting factor in detecting PSMs. This was addressed in this study by defining the minimum positive area (2.56 mm$^2$, corresponding to 4 × 4 voxels) based on the spatial resolution for $^{18}$F on this scanner that allowed for reliable macroscopic PSM detection (*36*). Detection of microscopic PSMs remains a technical challenge. A promising CT-based machine-learning segmentation approach was recently used for nodal segmentation in a pilot investigation and could further facilitate microscale segmentation in ex vivo PET/CT imaging (*43*). Several deep learning–assisted PET or PET/CT fusion segmentation techniques could also be explored (*44,45*). Alternative intraoperative techniques include ex vivo confocal microscopy and PSMA-coupled fluorophores. These technologies can offer valuable real-time or near-real-time feedback on assessment of surgical margins during surgery (*46*).

Radioguided surgery using positron emitters benefits from less attenuation of the high-energy 511 keV photons within the resected tissue when compared with γ-emitters, hence increasing the available signal for investigations of the activity distribution. In this study, we used [$^{18}$F]PSMA-1007 that has additional advantages over $^{68}$Ga-PSMA tracers. $^{18}$F has a lower positron energy, which increases image quality and spatial resolution—a key factor in margin assessment. The overall spatial resolution was reported to be 1.8 mm for $^{18}$F compared with 3.2 mm for $^{68}$Ga (*36*). Further, its longer physical half-life allowed for intraoperative imaging 2–4 half-lives after administration. For the same clinical setup, this would translate to 4–6 $^{68}$Ga half-lives and correspondingly lower signal intensity. Besides physical properties, [$^{18}$F]PSMA-1007 is primarily eliminated via the hepatobiliary

excretion route, which also potentially decreases the risk of radioactive contamination of the prostate bed from bladder activity during resection (*29*).

Several limitations are associated with our study. The power of the analyses was limited by the small number of patients. In addition, the current study design does not allow for direct comparison of [$^{18}$F]PSMA-1007 and $^{68}$Ga-PSMA tracers. Lastly, as of March 2024, there was, except for 1 patient, no evidence of biochemical or local recurrence in our patient cohort to allow for further investigations of predictive markers from our data. Prospective trials and a longer follow-up period are needed to validate our results and to assess the added value of PSMA-based ex vivo PET/CT guidance in RP.

## CONCLUSION

We demonstrated that intraoperative ex vivo PET/CT with iterative thresholding is highly accurate, sensitive, and specific (up to 94%, 83%, and 100%, respectively) in detecting positive resection margins in intraprostatic lesions and could be used to guide RP in high-risk PC patients. However, detection is limited to macroscopic PSMA-positive tumor foci. For margin assessment, we recommend the administration of at least 0.4 and 1.9 MBq/kg of [$^{18}$F]PSMA-1007 for intraoperative and preoperative injections, respectively. Prospective trials are needed to validate our results and to assess the added value of PSMA-based ex vivo PET/CT guidance in RP.

## DISCLOSURE

All disclosures listed were unrelated to the submitted work. Walter Jentzen received research funding from Siemens Healthineers. David Kersting received research funding from the German Research Association (DFG) and Pfizer, and speaker honoraria from Novartis and Pfizer. Henning Reis received research funding from Bristol-Myers Squibb, and consultation or speaker honoraria from Roche, Bristol-Myers Squibb, Janssen-Cilag, Novartis, Astra-Zeneca, MCI, CHOP GmbH, Sanofi, Boehringer Ingelheim, GlaxoSmithKline, Merck, Diaceutics, and HUeG and Evidia GmbH. Claudia Kesch received research funding from AAA/Novartis, Amgen, and Mariana Oncology; consulting honoraria from Apogepha, speaker honoraria from Novartis and Pfizer; and travel support from Janssen R&D, Amgen, and Bayer. Ulrich Krafft received research grants from BMS and AAA/Novartis, and personal fees from Janssen, Flatiron, MSD, and Intuitive Surgical. Boris Hadaschik received research grants from DFG, Novartis, and BMS; holds royalties from Uromed; received consulting fees from Novartis, BMS, and MSD/Pfizer; and received consulting fees and speaker honoraria from Janssen, Bayer, Amgen, Astellas, and AstraZeneca. Ken Herrmann reports personal fees from Bayer, SIRTEX, Adacap, Curium, Endocyte, IPSEN, Siemens Healthineers, GE HealthCare, Amgen, Novartis, ymabs, Aktis Oncology, Theragnostics, Pharma15, Debiopharm, AstraZeneca, and Janssen; personal fees and other from SOFIE Biosciences; nonfinancial support from ABX; and grants and personal fees from BTG. Wolfgang Fendler received research funding from SOFIE Biosciences; research funding, consulting, and speaker honoraria from Bayer; consulting and speaker honoraria from Janssen and Novartis; consulting honoraria from Calyx; and speaker honoraria from Telix, GE HealthCare, Eczacıbaşı Monrol, ABX, Amgen, and Urotrials. Christopher Darr reports personal fees from Janssen-Cilag and Ipsen, and travel fees from Janssen-Cilag, Ipsen, and Bayer. No other potential conflict of interest relevant to this article was reported.

**KEY POINTS**

**QUESTION:** Is surgical margin detection with intraoperative ex vivo PET/CT feasible in high-risk PC patients undergoing RP?

**PERTINENT FINDINGS:** Intraoperative ex vivo PET/CT shows a high sensitivity (83%), specificity (100%), and positive and negative predictive values (100% and 92%, respectively) with regards to detection of PSMs in excised prostate glands after RP.

**IMPLICATIONS FOR PATIENT CARE:** Intraoperative ex vivo PET/CT may contribute to the management of high-risk PC via intraoperative margin assessment.

## REFERENCES

1. Sung H, Ferlay J, Siegel RL, et al. Global cancer statistics 2020: GLOBOCAN estimates of incidence and mortality worldwide for 36 cancers in 185 countries. *CA Cancer J Clin.* 2021;71:209–249.
2. James ND, Tannock I, N'Dow J, et al. The Lancet Commission on prostate cancer: planning for the surge in cases. *Lancet.* 2024;403:1683–1722.
3. EAU Guidelines. Edn. presented at the EAU Annual Congress Paris 2024. ISBN 978-94-92671-23-3.
4. Martini A, Gandaglia G, Fossati N, et al. Defining clinically meaningful positive surgical margins in patients undergoing radical prostatectomy for localised prostate cancer. *Eur Urol Oncol.* 2021;4:42–48.
5. Iczkowski KA, Lucia MS. Frequency of positive surgical margin at prostatectomy and its effect on patient outcome. *Prostate Cancer.* 2011;2011:673021.
6. Petralia G, Musi G, Padhani AR, et al. Robot-assisted radical prostatectomy: multiparametric MR imaging-directed intraoperative frozen-section analysis to reduce the rate of positive surgical margins. *Radiology.* 2015;274:434–444.
7. Gordon IO, Tretiakova MS, Noffsinger AE, Hart J, Reuter VE, Al-Ahmadie HA. Prostate-specific membrane antigen expression in regeneration and repair. *Mod Pathol.* 2008;21:1421–1427.
8. Kasperzyk JL, Finn SP, Flavin R, et al. Prostate-specific membrane antigen protein expression in tumor tissue and risk of lethal prostate cancer. *Cancer Epidemiol Biomarkers Prev.* 2013;22:2354–2363.
9. Gondoputro W, Scheltema MJ, Blazevski A, et al. Robot-assisted prostate-specific membrane antigen-radioguided surgery in primary diagnosed prostate cancer. *J Nucl Med.* 2022;63:1659–1664.
10. Gandaglia G, Mazzone E, Stabile A, et al. Prostate-specific membrane antigen radioguided surgery to detect nodal metastases in primary prostate cancer patients undergoing robot-assisted radical prostatectomy and extended pelvic lymph node dissection: results of a planned interim analysis of a prospective phase 2 study. *Eur Urol.* 2022;82:411–418.
11. Jilg CA, Reichel K, Stoykow C, et al. Results from extended lymphadenectomies with [$^{111}$In]PSMA-617 for intraoperative detection of PSMA-PET/CT-positive nodal metastatic prostate cancer. *EJNMMI Res.* 2020;10:17.
12. Mix M, Schultze-Seemann W, von Büren M, et al. $^{99m}$Tc-labelled PSMA ligand for radio-guided surgery in nodal metastatic prostate cancer: proof of principle. *EJNMMI Res.* 2021;11:22.
13. Maurer T, Robu S, Schottelius M, et al. $^{99m}$Technetium-based prostate-specific membrane antigen-radioguided surgery in recurrent prostate cancer. *Eur Urol.* 2019;75:659–666.
14. Koehler D, Sauer M, Klutmann S, et al. Feasibility of $^{99m}$Tc-MIP-1404 for SPECT/CT imaging and subsequent PSMA-radioguided surgery in early biochemically recurrent prostate cancer: a case series of 9 patients. *J Nucl Med.* 2023;64:59–62.
15. Mancini-Terracciano C, Donnarumma R, Bencivenga G, et al. Feasibility of beta-particle radioguided surgery for a variety of "nuclear medicine" radionuclides. *Phys Med.* 2017;43:127–133.
16. Camillocci ES, Baroni G, Bellini F, et al. A novel radioguided surgery technique exploiting $\beta^-$ decays. *Sci Rep.* 2014;4:4401.
17. Fragoso Costa P, Shi K, Holm S, et al. Surgical radioguidance with beta-emitting radionuclides; challenges and possibilities: a position paper by the EANM. *Eur J Nucl Med Mol Imaging.* 2024;51:2903–2921.
18. Collamati F, van Oosterom MN, De Simoni M, et al. A DROP-IN beta probe for robot-assisted $^{68}$Ga-PSMA radioguided surgery: first ex vivo technology evaluation using prostate cancer specimens. *EJNMMI Res.* 2020;10:92.

19. Darr C, Fragoso Costa P, Kesch C, et al. Prostate specific membrane antigen-radio guided surgery using Cerenkov luminescence imaging-utilization of a short-pass filter to reduce technical pitfalls. *Transl Androl Urol.* 2021;10:3972–3985.
20. Olde Heuvel J, de Wit-van der Veen BJ, van der Poel HG, et al. $^{68}$Ga-PSMA Cerenkov luminescence imaging in primary prostate cancer: first-in-man series. *Eur J Nucl Med Mol Imaging.* 2020;47:2624–2632.
21. Heuvel JO, de Wit-van der Veen BJ, van der Poel HG, et al. Cerenkov luminescence imaging in prostate cancer: not the only light that shines. *J Nucl Med.* 2022; 63:29–35.
22. Darr C, Harke NN, Radtke JP, et al. Intraoperative $^{68}$Ga-PSMA Cerenkov luminescence imaging for surgical margins in radical prostatectomy: a feasibility study. *J Nucl Med.* 2020;61:1500–1506.
23. Costa PF, Pullen L, Kesch C, et al. $^{18}$F-PSMA Cerenkov luminescence and flexible autoradiography imaging in a prostate cancer mouse model and first results of a radical prostatectomy feasibility study in men. *J Nucl Med.* 2023;64:598–604.
24. Fendler WP, Calais J, Eiber M, et al. Assessment of $^{68}$Ga-PSMA-11 PET accuracy in localizing recurrent prostate cancer: a prospective single-arm clinical trial. *JAMA Oncol.* 2019;5:856–863.
25. Hofman MS, Lawrentschuk N, Francis RJ, et al.; proPSMA Study Group Collaborators. Prostate-specific membrane antigen PET-CT in patients with high-risk prostate cancer before curative-intent surgery or radiotherapy (proPSMA): a prospective, randomised, multicentre study. *Lancet.* 2020;395:1208–1216.
26. Mottet N, van den Bergh RCN, Briers E, et al. EAU-EANM-ESTRO-ESUR-SIOG guidelines on prostate cancer—2020 update. Part 1: screening, diagnosis, and local treatment with curative intent. *Eur Urol.* 2021;79:243–262.
27. Muraglia L, Mattana F, Travaini LL, et al. First live-experience session with PET/CT specimen imager: a pilot analysis in prostate cancer and neuroendocrine tumor. *Biomedicines.* 2023;11:645.
28. Darr C, Costa PF, Kahl T, et al. Intraoperative molecular positron emission tomography imaging for intraoperative assessment of radical prostatectomy specimens. *Eur Urol Open Sci.* 2023;54:28–32.
29. Kesch C, Vinsensia M, Radtke JP, et al. Intraindividual comparison of $^{18}$F-PSMA-1007 PET/CT, multiparametric MRI, and radical prostatectomy specimens in patients with primary prostate cancer: a retrospective, proof-of-concept study. *J Nucl Med.* 2017;58:1805–1810.
30. Giesel FL, Hadaschik B, Cardinale J, et al. F-18 labelled PSMA-1007: biodistribution, radiation dosimetry and histopathological validation of tumor lesions in prostate cancer patients. *Eur J Nucl Med Mol Imaging.* 2017;44:678–688.
31. Kim M, Seifert R, Fragemann J, et al. Evaluation of thresholding methods for the quantification of [$^{68}$Ga]Ga-PSMA-11 PET molecular tumor volume and their effect on survival prediction in patients with advanced prostate cancer undergoing [$^{177}$Lu]Lu-PSMA-617 radioligand therapy. *Eur J Nucl Med Mol Imaging.* 2023;50: 2196–2209.
32. Seifert R, Herrmann K, Kleesiek J, et al. Semiautomatically quantified tumor volume using $^{68}$Ga-PSMA-11 PET as a biomarker for survival in patients with advanced prostate cancer. *J Nucl Med.* 2020;61:1786–1792.
33. Draulans C, De Roover R, van der Heide UA, et al. Optimal $^{68}$Ga-PSMA and $^{18}$F-PSMA PET window levelling for gross tumour volume delineation in primary prostate cancer. *Eur J Nucl Med Mol Imaging.* 2021;48:1211–1218.
34. Mittlmeier LM, Brendel M, Beyer L, et al. Feasibility of different tumor delineation approaches for $^{18}$F-PSMA-1007 PET/CT imaging in prostate cancer patients. *Front Oncol.* 2021;11:663631.
35. Seifert R, Emmett L, Rowe SP, et al. Second version of the prostate cancer molecular imaging standardized evaluation framework including response evaluation for clinical trials (PROMISE V2). *Eur Urol.* 2023;83:405–412.
36. Moraitis A, Darr C, Kahl T, Pullen L. EANM'23 abstract book congress Sep 9–13, 2023. *Eur J Nucl Med Mol Imaging.* 2023;50(suppl 1):131.
37. Moraitis A, Kahl T, Jentzen W, et al. Molecular tumour volume segmentation in specimenPET/CT for intraoperative margin assessment in radical prostatectomy: a phantom study. Paper presented at: DGN Congress. 2024;63(suppl 2):149.
38. Jentzen W. An improved iterative thresholding method to delineate PET volumes using the delineation-averaged signal instead of the enclosed maximum signal. *J Nucl Med Technol.* 2015;43:28–35.
39. Trevethan R. Sensitivity, specificity, and predictive values: foundations, pliabilities, and pitfalls in research and practice. *Front Public Health.* 2017;5:307.
40. Foster B, Bagci U, Mansoor A, Xu Z, Mollura DJ. A review on segmentation of positron emission tomography images. *Comput Biol Med.* 2014;50:76–96.
41. Veluponnar D, de Boer LL, Geldof F, et al. Toward intraoperative margin assessment using a deep learning-based approach for automatic tumor segmentation in breast lumpectomy ultrasound images. *Cancers (Basel).* 2023;15:1652.
42. Luo L, Zheng A, Chang R, et al. Evaluating the value of $^{18}$F-PSMA-1007 PET/CT in the detection and identification of prostate cancer using histopathology as the standard. *Cancer Imaging.* 2023;23:108.
43. Rovera G, Grimaldi S, Oderda M, et al. Machine learning CT-based automatic nodal segmentation and PET semi-quantification of intraoperative $^{68}$Ga-PSMA-11 PET/CT images in high-risk prostate cancer: a pilot study. *Diagnostics (Basel).* 2023;13:3013.
44. Shiri I, Amini M, Yousefirizi F, et al. Information fusion for fully automated segmentation of head and neck tumors from PET and CT images. *Med Phys.* 2024;51: 319–333.
45. Yousefirizi F, Klyuzhin IS, O JH, et al. TMTV-Net: fully automated total metabolic tumor volume segmentation in lymphoma PET/CT images—a multi-center generalizability analysis. *Eur J Nucl Med Mol Imaging.* 2024;51:1937–1954.
46. Windisch O, Diana M, Tilki D, Marra G, Martini A, Valerio M. Intraoperative technologies to assess margin status during radical prostatectomy–a narrative review. *Prostate Cancer Prostatic Dis.* 2024:1–8.